Combustion-Related Shear-Flow Dynamics in Elliptic Supersonic Jets

K. C. Schadow,* E. Gutmark,† S. Koshigoe,‡ and K. J. Wilson§
Naval Weapons Center, China Lake, California

An elliptic jet having an aspect ratio of 3 : 1 was studied and compared to a circular jet at three Mach numbers: $M = 0.15$, 1, and 1.3. Hot-wire measurements and schlieren photography were employed in this study. The superior mixing characteristics of an elliptic jet relative to a circular jet, which were found in previous works on subsonic jets, prevail in the sonic jet and are further augmented by the shock structures of the supersonic underexpanded jet. The major and minor axes switch at a distance of 3 diameters from the nozzle, and the spreading rate of the minor axis side is twice that of a subsonic jet. The experimental data are supported by results of the linear instability analysis of the supersonic elliptic jet. This analysis shows that the initial vortices are bending at the major axis side in a process similar to that which occurs in a subsonic elliptic jet.

Introduction

IN reacting flows, the flame stability and heat release are closely related to the interaction between fluid dynamics and combustion. Specifically in a dump combustor, with a flowfield of a ducted jet with dump, the combustion is related to the dynamics of the shear flow originating at the jet exit of the dump.

The evolution of subsonic shear layers, associated with vortex shedding and interaction, has been studied by many investigators both experimentally[1-3] and analytically.[4] These studies, which have recognized the important role of large-scale structures, have opened up the possibility of modifying actively or passively the regular breakdown of large-scale vortices into fine-scale turbulence.[5,6] One method of passive shear-flow control was obtained using noncircular jet-exit cross sections, which change the initial conditions of the jet. Noncircular jets did not attract the interest of researchers, and only a few studies with triangular and rectangular jets were reported in the literature.[7,8]

Another noncircular nozzle configuration that was investigated was the small aspect ratio elliptic nozzle.[9] Compared to regular circular jets, the entrainment into the elliptic jet was significantly enhanced in subsonic, nonreacting freejet and ducted-jet tests at low and high Reynolds numbers.[10-14] Primarily responsible for the mixing enhancement is the phenomenon of axis switching, which occurs as a result of flow self-induction processes associated with the bending of the elliptic vortices.[15]

Moreover, the elliptic jet was superior to a circular jet in a subsonic fuel-rich plume combustion process where, in addition to the entrainment (bulk mixing) of reactants, mixing on the fine-scale (molecular scale) is important.[16] The intense fine-scale activity in the shear layer was due to the generation of azimuthal modes of instability that were excited by the noncircular initial conditions.[11,17,18] Evidence exists that supersonic shear-flow dynamics are also governed by large-scale structures,[19-22] a feature that would allow passive shear-flow control in supersonic combustion.

The objective of the present work is to determine whether the special entrainment features of subsonic elliptic jets can also be found in sonic and supersonic freejets. This combined experimental and analytical work provides a basis for future supersonic ducted flow and combustion research.

Experiments were performed with cold and heated freejets in both fully expanded and underexpanded conditions using hot-wire anemometry, thermocouples, and schlieren photography. The theoretical part includes stability analysis of circular and elliptic jets using an integral-equation formulation of the linear stability analysis that is applicable to arbitrary cross sections.[23]

Experimental Setup

In the nonreacting tests, air from a blowdown facility was supplied to a freejet test setup with interchangeable circular and 3 : 1 aspect ratio elliptic nozzles having a diameter or equivalent diameter of $D = D_e = 18.4$ mm (Fig. 1). The measurements were carried out for three conditions: 1) a subsonic jet with exit velocity of $M = 0.15$, 2) a fully expanded jet with sonic velocity at the exit, and 3) an underexpanded jet having a Mach number of $M_j = 1.27$.

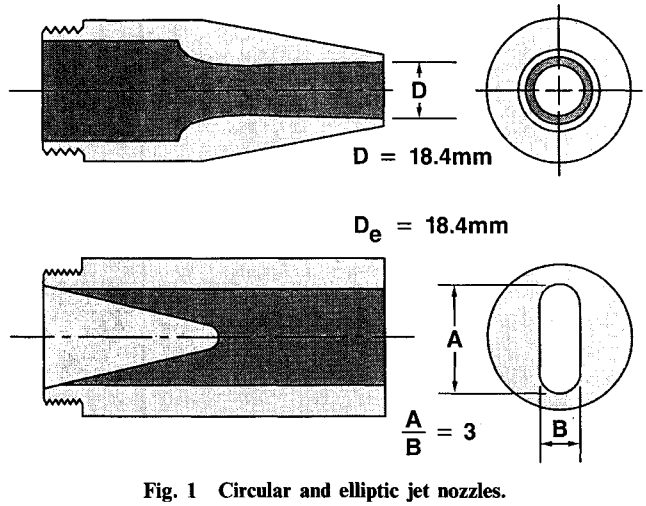

Fig. 1 Circular and elliptic jet nozzles.

Received Feb. 23, 1988, revision received Oct. 17, 1988.

*Supervisory General Engineer, Propulsion Research Branch, Engineering Sciences Division, Research Department.
†Research Scientist, Propulsion Research Branch, Engineering Sciences Division, Research Department.
‡Physicist, Propulsion Research Branch, Engineering Sciences Division, Research Department.
§Aerospace Engineer, Propulsion Research Branch, Engineering Sciences Division, Research Department.

The tests were performed in an air-conditioned laboratory with a temperature of 20°C ± 0.5°C. The jet was mounted at least 5 ft from any solid surface, and the surfaces were covered with sound absorbing foam to eliminate any possible reflection that could affect the jet spread.

The mean and turbulent velocity fields of the jets were measured using a constant-temperature hot-wire anemometer with a frequency response of 80 kHz. An overheat ratio of 1.6 was used in the measurements. The wire was calibrated up to sonic velocity using a compressibility correction factor. No measurements were done in the supersonic region of the jet. The traversing grid was selected to measure only in the lower-than-sonic regions of the flow to reduce the possibility of wire breakage and avoid the problem of supersonic calibration.

The hot wire was mounted on a computer-controlled precise traverse mechanism enabling movement in all three axes. A typical measurement included 500 points covering the entire jet from the nozzle to 30 equivalent diameters downstream of the exit.

A 3-mm-diam B&K microphone was used to determine the power spectra of the near-field pressure fluctuations at the potential core region. The microphone had a frequency response of up to 140 kHz. Details of the experimental procedure are given in Ref. 24. Schlieren photography was used to visualize the shock structures of the circular and elliptic nozzles.

In the reacting tests, the circular and elliptic nozzles were mounted at the exit of a dump combustor burning a lean mixture of air and hydrocarbon fuel at $P = 650$ kPa and $T = 1400$ K. Color photos were made of the exhaust shock pattern. In addition, mean temperatures in the exhaust jet were measured using a rake of eight tungsten/rhenium-thermocouples. The hot-wire, thermocouples, and microphone calibration data acquisition and analysis were done using a VAX-750 minicomputer.

Results and Discussion

The phenomenon of axis switching in a subsonic three-dimensional elliptic jet was reported in previous works[7,9] and is shown in Fig. 2 as a reference for the present experimental setup. The spreading rate of the jet in the minor axis plane was higher than that in the major axis plane. The major and minor sides of the initially 3 : 1 aspect ratio jet became equal at $x/D_e = 23$. This crossover point was previously shown to be a function of the nozzle aspect ratio and jet exit velocity. The spreading rate of the elliptic jet is compared to that of a circular jet. The spreading rate at the minor axis plane of the jet is larger than that of the circular jet at $x/D_e < 5$ and $x/D_e > 20$. In the other section it is similar in the two jets. This particular behavior of the elliptic jet is a result of the self-induction of the asymmetric coherent structures. The coherent structures undergo azimuthal distortion due to the Kelvin-Helmholtz instability, and consequently the self-induction process is enhanced. The instability process of the subsonic and supersonic jet flows is discussed briefly in the following section to elucidate the basic differences and similarities of the two flows, especially regarding their spreading rates.

Instability Analysis of Elliptic Jets

An integral-equation formulation of the linear stability analysis was developed for jets with arbitrary shapes.[23] Using this method, the stability characteristics of elliptic jets were studied for different aspect ratios and Mach numbers.

Figure 3 describes the dependence of the spatial growth rates ($-\alpha_i$) of disturbances in the initial circular jet shear layer and their phase velocity (C_p) on the frequency of these disturbances at different Mach numbers. The growth rates diminished with increasing Mach number at subsonic flow ($M = 0$), $\alpha_i R_e = -5.6$ (where R_e is the jet equivalent radius), while at supersonic flow ($M = 1.5$), $\alpha_i R_e = -2$. The most amplified frequencies, corresponding to the peak values of the

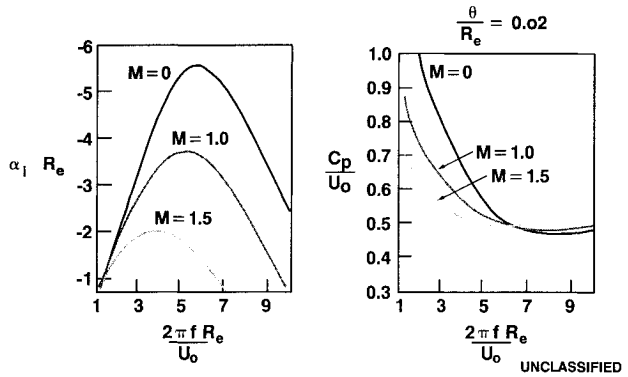

Fig. 3 Growth rate and phase velocity as function of frequency for axisymmetric mode of circular jet at different Mach numbers.

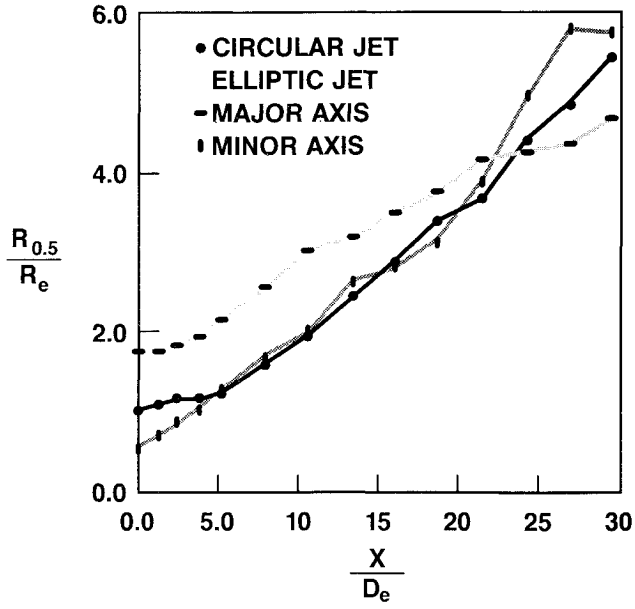

Fig. 2 Comparison of jet spread for circular and elliptic jets—Mach 0.15.

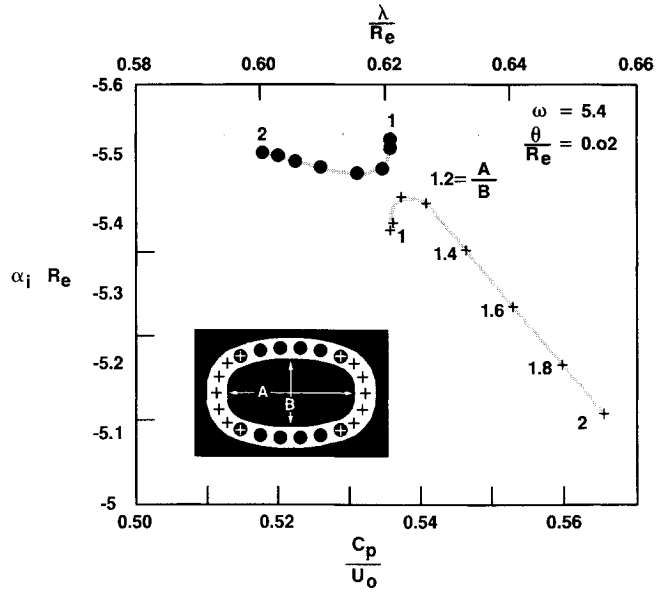

Fig. 4 Variation of growth rate, wavelength, and phase velocity as function of aspect ratio for the two major components of first azimuthal mode at Mach 0.

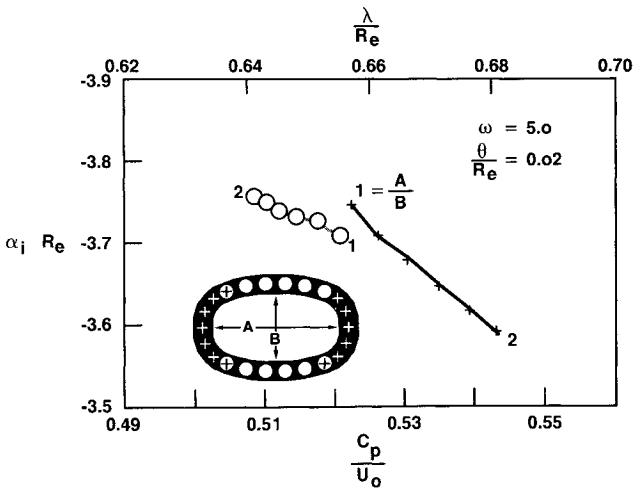

Fig. 5 Variation of growth rate, wavelength, and phase velocity as function of aspect ratio for the two major components of first azimuthal mode at Mach 1.0.

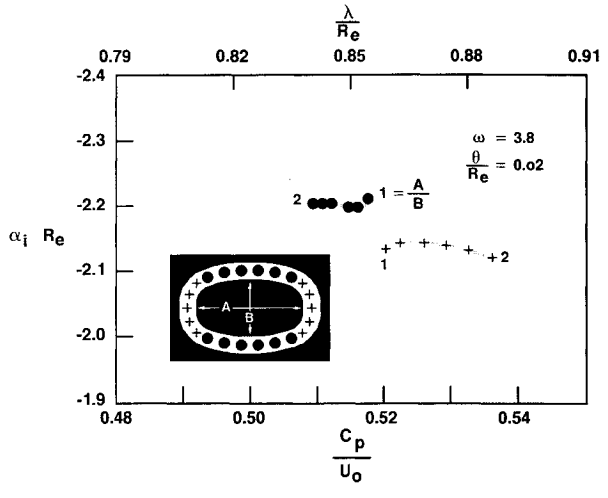

Fig. 6 Variation of growth rate, wavelength, and phase velocity as function of aspect ratio for the two major components of first azimuthal mode at Mach 1.5.

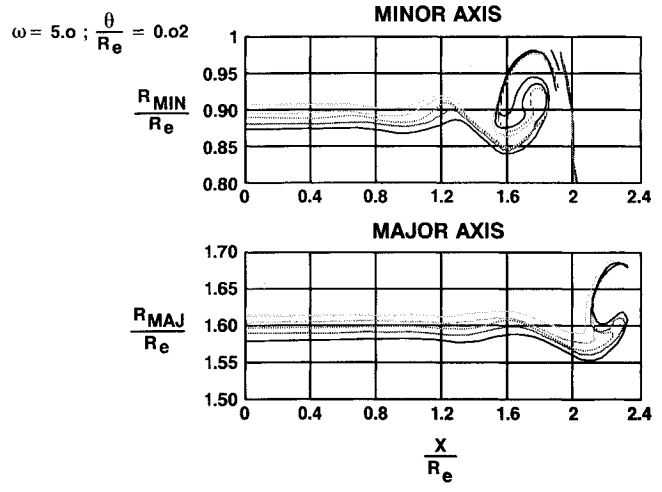

Fig. 7 Streaklines for vortex rollup at major and minor axes for 2 : 1 elliptic jet at Mach 1.0.

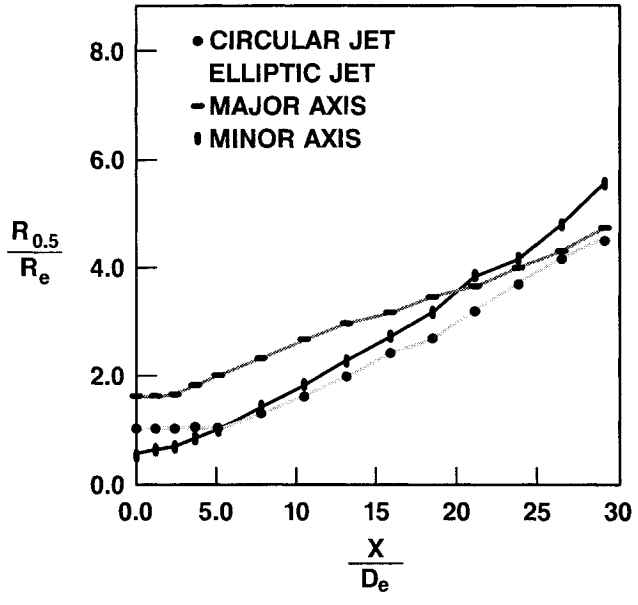

Fig. 8 Comparison of jet spread for circular and elliptic jets—Mach 1.0.

growth rates, decreased with increasing Mach number. The nondispersive range of the frequencies, i.e., the range of frequencies that move at the same phase velocity, was wider for higher Mach numbers.

When the jet eccentricity was varied from a circular jet to an elliptic jet with different aspect ratios, the growth rate and the phase velocity of the amplified waves were also changed. The noncircular jet stability characteristics were also associated with various azimuthal modes. These modes represent a variation of the disturbance amplitude and phase around the jet circumference. Figure 4 shows the variation of the growth rate and phase velocity as a function of the aspect ratio A/B (where A is the major axis length of the jet nozzle and B is the minor axis length) for a subsonic flow ($M = 0$). The graph depicts the variation of the two main components of the first azimuthal mode. The insert to the figure shows that the first component, described by the circular symbols, was dominant in the jet section with the large radius of curvature (minor axis plane). The second component, described by the "plus" symbols, was dominant in the section having the small radius of curvature (major axis plane). When the jet eccentricity was varied from 1 (circular jet) to a 2 : 1 elliptic jet, the amplification rate of the first component was almost invariable, but its phase velocity was decreased from 0.54 to 0.52. With the same variation of eccentricity, the second component underwent a reduction of its amplification rate accompanied by an increase in the phase velocity from 0.54 to 0.57. The outcome of these changes was that the mode that is dominant at the major axis side moved faster than the one at the minor axis side. This differential motion caused bending of the jet coherent structures at the major axis side, initiating the self-induction process and the subsequent accelerated spreading rate of the minor axis section.

When the jet Mach number was increased to 1 (sonic jet), a similar behavior was observed (Fig. 5). Although the two components of the azimuthal eigenmode switched the center of their activity between the minor and major axis planes, the phase velocity of the unstable waves at the major axis was still high relative to the minor axis side. The same condition also occurred at supersonic speeds of $M = 1.5$ (Fig. 6).

The difference in the phase speed and amplification rates between the major and minor axis sides resulted in a different rollup location of the vortices at the two sides. The computed streaklines in Fig. 7 show that the rollup was completed in the minor axis sides at $x/R_e \approx 1.6$, while at the major axis side it occurred further downstream at $x/R_e \approx 2.4$. This pattern of nonsymmetric rollup resulted in vortex bending, which was also observed earlier in water flow visualizations.[12] The self-induction process ensuing from this bending yielded the high spreading rate typical of the elliptic jet. The stability analysis results, which were described earlier, suggest that the mecha-

nism that was found in subsonic flows also prevails in supersonic flows. In supersonic flows with shock structures, as in a jet operated at off-design conditions, there could be additional contribution from the shock/shear layer interaction. This interaction can lead to feedback loop, which was shown to enhance mixing.[25]

Sonic and Supersonic Axes Switching

The spreading rates of sonic elliptic and circular jets ($M = 1$) are compared in Fig. 8. As predicted by the stability analysis, the axes switching can be observed here too. The circular jet's spreading rate was reduced slightly relative to the low subsonic case (Fig. 2), but the high spread of the minor axis section resulted in axes switching at $x/D_e = 20$, which is slightly upstream of the subsonic switching point.

When the jet's chamber pressure was further increased, an underexpanded jet was obtained. The jet Mach number following the initial expansion waves was $M_j = 1.3$. At this condition, the jet initial core was dominated by expansion-compression wave cell structures and its acoustic radiation concentrated in a narrow frequency peak called the jet screech frequency.[21,22] Figure 9 shows the power spectrum of the near-field pressure fluctuations of the underexpanded jet with $M_j = 1.3$. The screech frequency is close to 7000 Hz, with a power level of three orders of magnitude above the other broadband frequency components. Details on the near-field pressure fluctuations of this underexpanded jet are given in Ref. 24. This reference also describes the hot-wire spectral data in the jet shear layer relating the shear-layer instability frequencies to the near-field pressure fluctuations.

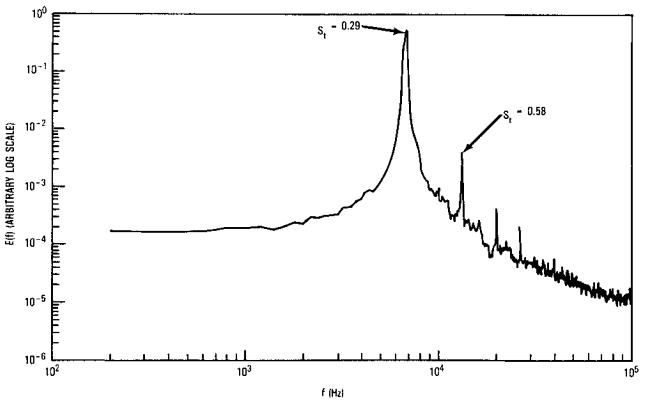

Fig. 9 Power spectrum of the near-field pressure fluctuations of underexpanded circular jet.

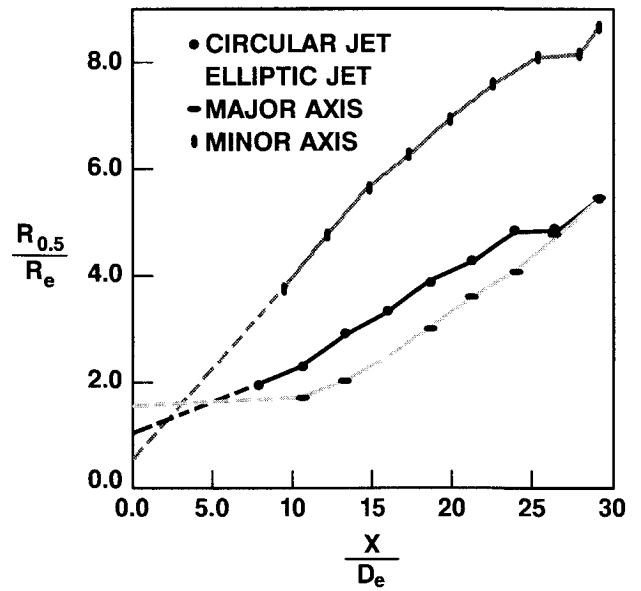

Fig. 10 Comparison of jet spread for circular and elliptic jets—Mach 1.3.

The shock structure of the underexpanded jet has a substantial effect on its spreading rate (Fig. 10). The spreading rate of the minor axis side was doubled relative to the sonic jet, while the width at the major axis side remained unchanged until $x/D_e = 10$. From this point, its growth was similar to that of the circular jet. The axes switching location was moved far upstream to $x/D_e \approx 3$.

Axes switching in the elliptic jet is further enhanced relative to a circular jet in the supersonic regime due to mode switching. The subsonic and sonic circular and elliptic jets are predominantly symmetric. At low supersonic speeds the helical mode of the circular jet[26] and the flapping mode of the elliptical jet become dominant. This modal change increases the spreading rate of both jets at the Mach number range of $1.1 \leq M_j \leq 1.4$. The interaction between the shocks and flapping mode of the elliptic jet makes this change more pronounced.[27]

The rapid occurrence of the axes switching in the underexpanded jet is also shown in Fig. 11 for an elliptic underexpanded reacting jet. The second shock cell has its wider dimension aligned in the minor axis plane and its narrow one in the major axis plane. Temperature measurements done in this elliptic underexpanded jet showed the larger width of the jet at the minor axis plane relative to the other plane at a distance of $x/D_e = 8$ (Fig. 12). The thermal image of the circular jet is compared with the major and minor planes of the noncircular jet (Fig. 13). The thermal images show the high spreading of the jet at the minor axis plane, relative to the narrowing of the jet in the other plane, resulting in axes

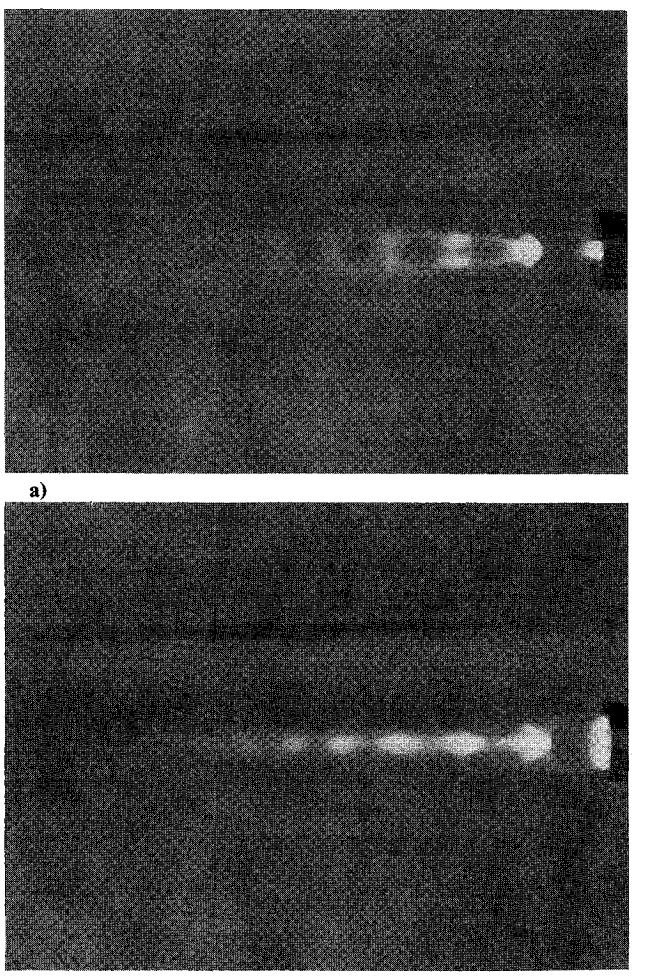

Fig. 11 Elliptic underexpanded reacting jet: a) minor axis; b) major axis.

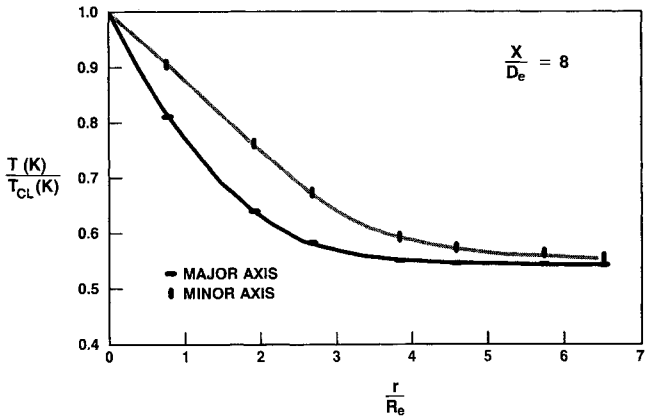

Fig. 12 Comparison of radial temperature profiles in circular jet and elliptic jet.

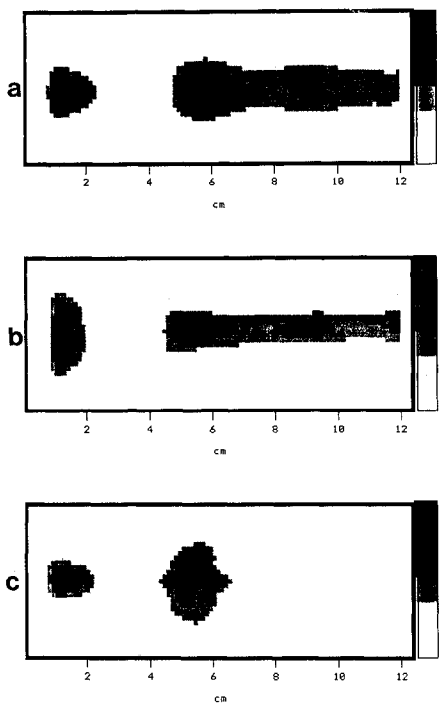

Fig. 13 Thermal images of the a) circular, b) major plane, and c) minor plane for supersonic combustion ($M_j = 2$).

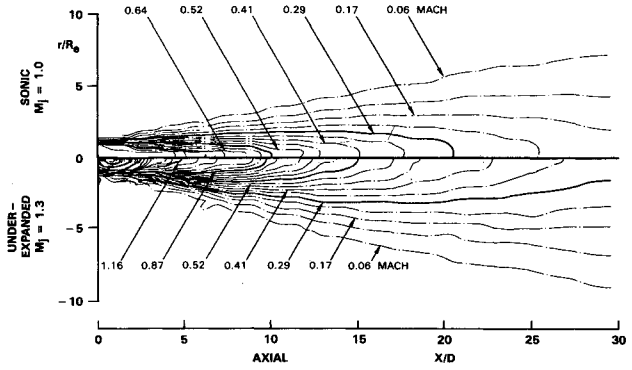

Fig. 14 Comparison of mean axial velocity contours—circular jet.

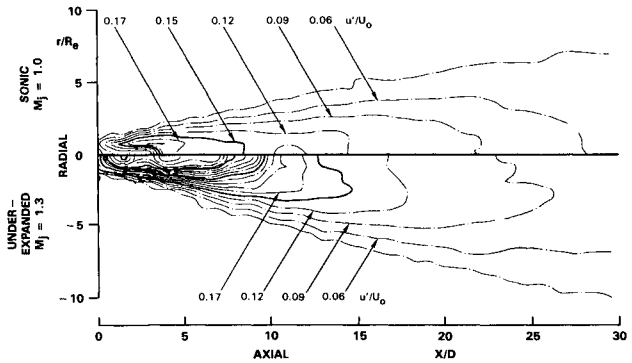

Fig. 15 Comparison of turbulent axial velocity contours—circular jet.

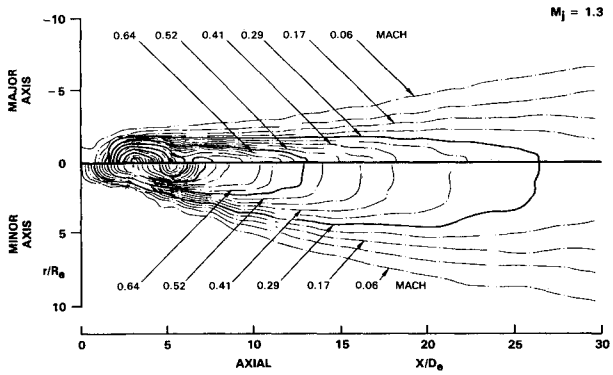

Fig. 16 Comparison of mean velocity contours—elliptic jet (underexpanded).

switching. The total mixing rate of this jet relative to the circular one for these conditions was significantly higher.

Mean and Turbulent Velocity Field

The mean velocity and turbulent axial velocity contours of the sonic ($M = 1$) and supersonic ($M = 1.3$) jets are shown in Figs. 14 and 15, respectively. The region of the supersonic jet core with shock structures was not covered by the hot-wire measurements. The contours in this area are drawn by the computer interpolation procedure. Both figures show that the supersonic jet spreads faster than the sonic jet. The turbulent intensity was higher for the supersonic jet and covered larger sections of the jet.

The mean and turbulent velocity contours on the major and minor axis planes of the underexpanded elliptic jet ($M_j = 1.3$) are shown in Figs. 16 and 17, respectively. The high spreading rate on the minor axis plane is evident. The jet width at the major axis plane remains almost constant in the first 10 diameters, and its spreading rate further downstream is small. Because of the lack of hot-wire data, the interpolation procedure resulted in a mismatch of the velocity contours at the centerline.

The cells formed by the expansion-compression waves structures inside the jet core, which could not be measured using the hot-wire, were visualized by schlieren photography. Figure 18 shows these structures in the underexpanded circular and elliptic jets. The nonsymmetric shape of the expansion/compression waves in the elliptic jet resulted in a different pattern of flow spread along the two axes of the jet. The intersection of the waves bouncing from the jet boundary were nonsymmetric and distorted.

The centerline velocity decay rates of the circular and elliptic jets are compared in Fig. 19. For $x/D_e > 10$, both jets had similar centerline deceleration rates for the three Mach numbers studied. The potential core length of the elliptic jet was very short, even for subsonic exit velocity. The core of the subsonic circular jet was 5 diameters long and decreased at the sonic speed. No measurements were taken for the supersonic jet in this region.

The centerline turbulence intensity of the circular and elliptic jets is shown in Fig. 20 for subsonic, sonic, and supersonic speeds. The turbulence intensity is amplified faster in the elliptic jet core than in the circular jet, both in subsonic and sonic velocities. Downstream of the core region both jets have

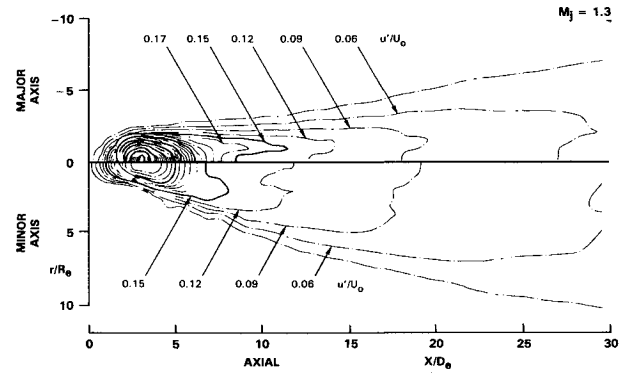

Fig. 17 Comparison of turbulent axial velocity contours—elliptic jet (underexpanded).

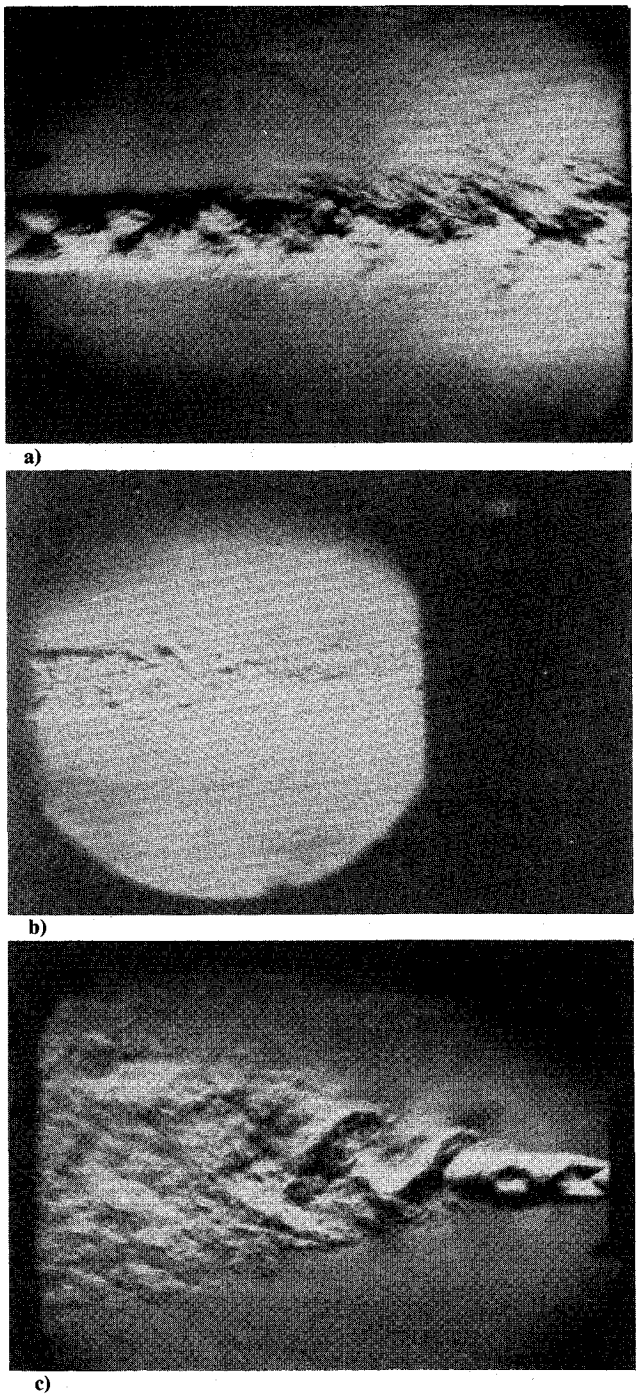

Fig. 18 Schlieren photographs of the underexpanded jets: a) circular jet; b) elliptic jet—major, 5 ns exposure; c) elliptic jet—minor, 5 ns exposure.

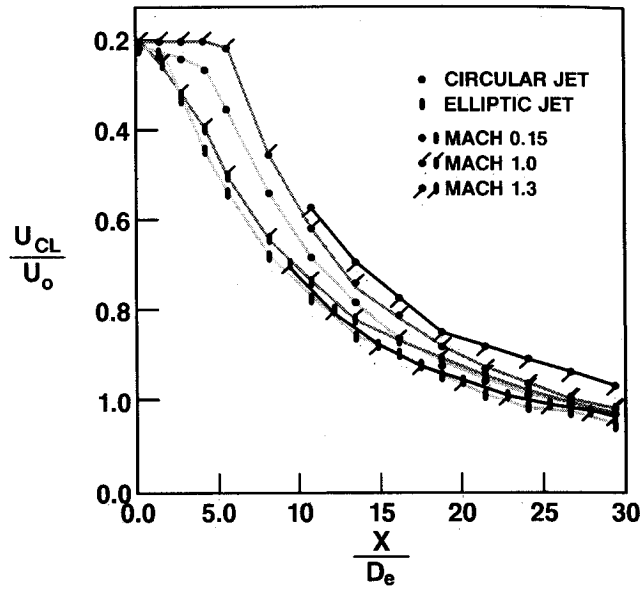

Fig. 19 Comparison of centerline velocity decay for circular and elliptic jets at three Mach numbers.

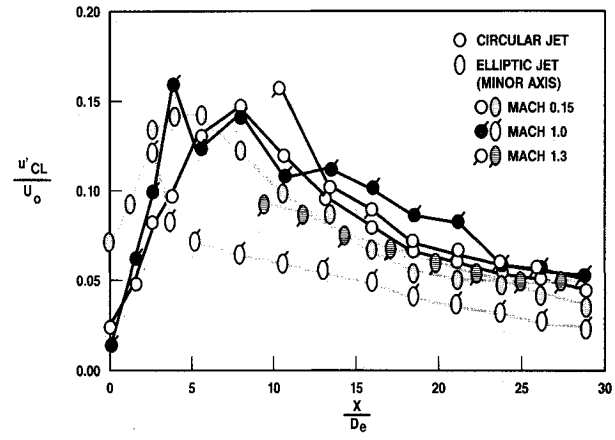

Fig. 20 Comparison of centerline turbulence for circular and elliptic jets at three Mach numbers.

nearly the same turbulence intensity for subsonic and supersonic exit Mach numbers. At sonic speed the circular jet has the highest intensity while the elliptic jet has the lowest.

Conclusions

The high rate of entrainment of the small aspect ratio elliptic jet relative to an axisymmetric or plane jet was attributed to a growth mechanism that does not exist in symmetric jets. This entrainment mechanism is related to the self-induction of vortices that are being distorted due to the variation of their instability characteristics around their circumference. It was shown here that although the distribution of the various eigenmodes changes from subsonic to supersonic jets, the initial vortical structures of the elliptic jet at the major axis plane bend in the streamwise direction relative to the minor axis section. This phenomenon also occurs in subsonic flows. Consequently, the self-induction of the jet coherent structures augments the amount of surrounding fluid engulfed by the jet at the minor axis section in the subsonic and sonic elliptic jets.

In a supersonic underexpanded elliptic jet, the series of bouncing expansion and compression waves generate a nonsymmetric structure of cells. The angles of the oblique shocks and expansion fans are different in the two planes of the jet, and the flow changes direction in a nonsymmetric pattern.

The experimental data described in the paper show the large increase of the spreading rate of this jet in the minor axis plane relative to the sonic and subsonic jets. The two axes switch direction at $x/D_e = 3$ instead of $x/D_e \approx 20$ in the lower-velocity jets. The interaction between the shock cells and the coherent structures of the jet shear layer is currently being studied in our laboratory.

References

[1]Crow, S. C. and Champagne, F. H., "Orderly Structure in Jet Turbulence," *Journal of Fluid Mechanics*, Vol. 48, 1971, pp. 547–591.

[2]Brown, G. L. and Roshko, A., "On Density Effects and Large Structures in Turbulent Mixing Layers," *Journal of Fluid Mechanics*, Vol. 64, No. 4, 1974, pp. 775–816.

[3]Ho, C. M. and Huerre, P., "Perturbed Free Shear Layers," *Annual Review of Fluid Mechanics*, Vol. 16, 1984, pp. 365–424.

[4]Michalke, A., "The Instability of Free Shear Layers," *Progress in Aerospace Science*, Vol. 12, Pergamon Press, Oxford, 1972, pp. 213–239.

[5]Hussain, A. K. M. F., "Coherent Structures and Turbulence," *Journal of Fluid Dynamics*, Vol. 173, 1986, pp. 303–356.

[6]Fiedler, H. E., "Coherent Structures," *Proceedings of the 1st European Turbulence Conference*, Lyon, 1986.

[7]Sforza, P. N., Steiger, M. H., and Trentacoste, N., "Studies on Three-Dimensional Viscous Jets," *AIAA Journal*, Vol. 4, April 1966, pp. 800–806.

[8]Trentacoste, N. and Sforza, P. N., "Further Experimental Results for Three-Dimensional Free Jets," *AIAA Journal*, Vol. 5, May 1967, pp. 885–891.

[9]Gutmark, E. and Ho, C. M., "Development of an Elliptic Jet," *Bulletin of Physical Society*, Vol. 27, No. 9, Nov. 1982, p. 1184.

[10]Schadow, K. C., Wilson, K. J., Lee, M. J., and Gutmark, E., "Enhancement of Mixing in Ducted Rockets With Elliptic Gas-Generator Nozzles," *Proceedings of the AIAA/SAE/ASME 20th Joint Propulsion Conference*, AIAA, New York. (Also the *Journal of Propulsion and Power*, Vol. 3, No. 2, March/April, 1987, pp. 145–149).

[11]Gutmark, E., Schadow, K. C., Parr, D. M., Harris, C. K., and Wilson, K. J., "The Mean and Turbulent Structure of Noncircular Jets," *Proceedings of the AIAA Shear Flow Control Conference*, AIAA Paper 85-0543, March 1985.

[12]Ho, C. M. and Gutmark, E., "Vortex Induction and Mass Entrainment in a Small Aspect Ratio Elliptic Jet," *Journal of Fluid Mechanics*, Vol. 179, 1987, pp. 383–405.

[13]Husain, H. S. and Hussain, A. K. M. F., "Controlled Excitation of Elliptic Jet," *Physics of Fluids*, Vol. 26, 1983, pp. 2763–2766.

[14]Schadow, K. C., Wilson, K. J., Parr, D. M., and Gutmark, E., "Mixing Characteristics of a Ducted, Elliptic Jet With Dump," *Journal of Propulsion and Power*, Vol. 4, No. 4, July/Aug. 1988, pp. 328–333.

[15]Dhanak, M. R. and De Bernardinis, B., "The Evolution of an Elliptic Vortex Ring," *Journal of Fluid Dynamics*, Vol. 109, 1981, pp. 189–216.

[16]Schadow, K. C., Gutmark, E., Parr, T. P., Parr, D. M., Wilson, K. J., and Ferrell, G. B., "Enhancement of Fine-Scale Mixing for Fuel-Rich Plume Combustion," AIAA Paper 87-0376, Jan. 1987.

[17]Gutmark, E. and Schadow, K. C., "Flow Characteristics of Orifice and Tapered Jets," *Physics of Fluids*, Vol. 30, Nov. 1987, pp. 3448–3454.

[18]Cohen, J., "Instabilities in Turbulent Free Shear Flows," D.Sc. Thesis, University of Arizona, Tucson, 1986.

[19]McLaughlin, D. K., Morrison, G. L., and Troutt, T. R., "Experiments on the Instability Waves in a Supersonic Jet and their Acoustic Radiation," *Journal of Fluid Mechanics*, Vol. 69, Part 1, 1975, pp. 73–95.

[20]Morrison, G. L. and McLaughlin, D. K., "Instability Process in Low Reynolds Number Supersonic Jets," *AIAA Journal*, Vol. 18, July 1980, pp. 793–800.

[21]Seiner, J. M., Manning, J. C., and Ponton, M. K., "The Preferred Spatial Mode of Instability for a Mach 2 Jet," AIAA Paper 86-1942, AIAA 10th Aeroacoustics Conference, Seattle, WA, 1986.

[22]Lepicovsky, J., Ahuja, K. K., Brown, W. H., and Burrin, R. H., "Coherent Large Scale Structures in High Reynolds Number Supersonic Jet in Mach Number 1.4," AIAA Paper 86-1941, 1986.

[23]Koshigoe, S. and Tubis, A., "Wave Structures in Jets of Arbitrary Shape," *Physics of Fluids*, Vol. 29, No. 12, 1986, pp. 3982–3992.

[24]Gutmark, E., Schadow, K. C., Wilson, K. J., and Bicker, C. J., "Acoustic Radiation and Flow Instabilities in Low Supersonic Circular and Elliptic Jets," *Physics of Fluids*, Vol. 31, No. 9, Sept. 1988, pp. 2524–2532.

[25]Glass, D. K., "Effects of Acoustic Feedback on the Spread and Decay of Supersonic Jets," *AIAA Journal*, Vol. 9, Oct. 1968, pp. 1890–1897.

[26]Gutmark, E., Schadow, K. C., and Bicker, C. J., "Mode Switching in Supersonic Circular Jets," *Physics of Fluids*, Vol. 1, No. 5, May 1989, pp. 868–873.

[27]Gutmark, E., Koshigoe, S., and Schadow, K. C., "Shock Wave/Shear Layer Interaction in Circular and Noncircular Jets," International Workshop on the Physics of Compressible Turbulent Mixing, Princeton, NJ, 1988.